12th Brazilian Congress of Manufacturing Engineering
May 10th-12th, 2023, Brasilia, DF, Brazil

EFFECT OF MICROSTRUCTURE ON MICROMILLING OF POWDER-BED-FUSED INCONEL 718

Jacob Southern
Texas A&M University, College Station, Texas, USA
jacob.southern@tamu.edu

James Hyder
KGSBO LLC, Katy, Texas, USA
jhyder@kgsbo.com

Mike Corliss
KGSBO LLC, Katy, Texas, USA
mcorliss@kgsbo.com

Jacob Galle
Texas A&M University, College Station, Texas, USA
jacobgalle@tamu.edu

Wayne NP Hung
Texas A&M University, College Station, Texas, USA
hung@tamu.edu

Abstract. *This paper studied micromilling of powder-bed-fused Inconel 718. Two scanning strategies (checkerboard, stripe), three cutting speeds (10, 14, 19 m/min), three chip loads (0.8, 1.0, 1.2 µm/tooth), and two tool coating (AlTiN/Si_3N_4, AlTiN) were selected for micromilling in minimum quantity lubrication with Ø0.5mm flat-end milling cutters. Both surface finish and width of micromilled slots were measured using a 3D digital microscope to determine the machinability of as-printed samples. Scanning electron microscopy and energy dispersive X-ray were used to examine the machined surface and identified different phases that may affect the machining process. Metallic carbide particles were formed due to fast cooling rate at the edges or corners of an Inconel block. Such hard particles damaged the fragile cutting edges and their thin coating layers, accelerated tool wear, and reduced the machined slot widths. After impact with a tool cutting edge, a carbide particle was either sheared off, shattered, or uprooted to smear on the machined surface along the tool path. The measured surface finish data were 100 times higher than theoretical values. Aggressive machining parameters using high cutting speed and /or chip load affected tool wear and reduced the slot width about 15 µm after 100 mm milling distance. The checkerboard scanning strategy, produced more consistent microstructure with even carbide particle distribution, resulted in more consistent surface finish and slot width data.*

Keywords: *Inconel 718, Additive Manufacturing; Micromilling; Tool wear; Intermetallic carbide; Surface finish; Slot width.*

1. INTRODUCTION

Inconel 718 (IN718) and other superalloys are commonly used in high stress and high temperature applications in nuclear, aerospace, energy, and machinery industries. Metal additive manufacturing, such as lases powder bed fusion (L-PBF), allows engineers to design and quickly fabricate prototypes of complex engineering components. Post processing after additive manufacturing is required to control surface finish, form, and dimensions of additively fabricated components. The published data on micromachining of additively manufactured IN718 are limited despite the popularity of IN718. Some researchers studied the effects of machining parameters on product quality but did not include the effect of printing parameters, scanning strategies, and microstructure of printed materials. The objectives of this study are to:

i) Investigate the effect of scanning strategies on microstructure of additively manufactured IN718,
ii) Study the effect of micromilling parameters and tool coatings for this superalloy.

2. LITERATURE REVIEW

2.1 Metal Additive Manufacture

Additive manufacturing is divided into seven classifications of processes. Each of these classifications have advantages and disadvantages that need to be evaluated when deciding which process to choose for the desired part. They are vat photopolymerization, powder bed fusion, binder jetting, material extrusion, material jetting, direct energy deposition and sheet lamination. Within each classification there is multiple technologies of additive manufacturing processes and each technology will have certain material limitations. Among those processes, material jetting, directed energy deposition and powder bed fusion are capable for metal printing (Gibson et al., 2015).

Material jetting is a process derived from the two-dimensional inkjet printers used in document printing. This process can be used to produce polymer, ceramic, or metallic parts (Gibson et al., 2015). Commonly, low melting temperature materials, such as tin-lead soldering alloy, are used with this technique. Material jetting is used in electronic applications for printing the traces, connections and soldering. The method for this process involves creating a droplet of liquid material that is deposited on the substrate using a printing head with multiple nozzles. Due to the multiple nozzles, this method is capable of printing more than just a single point at one instance of time allowing for this method to have decreased print time. The droplets are created with either the continuous mode or the drop-on-demand mode. The continuous mode leads to bigger droplets and low placement accuracy; therefore, the latter method is preferred. The method is accomplished by creating individual pressure pulses in the nozzles. Many machines use a piezoelectric actuator to create the pressure pulse to print a flat layer and then integrate those layers to form a three-dimensional (3D) part.

Directed energy deposition (DED) is a process that is predominately used with metal powders even though it has the capability of using polymers and ceramics (Gibson et al., 2015). Unlike the material jetting method, a wide range of metals is suitable for DED since low melting temperature is not required for manufacture of 3D part. The method uses a focused heat source to melt metal powder – or metallic wire – and then deposit the molten droplets through a moving nozzle. Laser or electron beam is the typical heat source used in DED system. Melting the powder as it is deposited allows DED system to repair or add features to an existing metallic part. However, this also limits the geometry of the part because of the lack of support structures in this method. Another disadvantage of this process is the stress that is induced from the rapid cooling as the heat source travels the part path. This thermally induced stress can lead to stress fractures within the part.

Another popular process for 3D metal manufacture is PBF that can utilize a wide range of metallic powders This process has four binding mechanisms including solid state sintering, liquid phase sintering, fully melting, and chemically induced binding from which the liquid phase sintering and fully melting are most common (Gibson et al., 2015). The processes that use these binding methods are called selective laser sintering (SLS) and selective laser melting (SLM) which is commonly referred to as L-PBF. The SLM, SLS, and L-PBF methods use a laser source to melt and bind the powder in an inert atmosphere. A high power density electron beam can be used in vacuum to achieve the similar effects. In these methods, a thin metallic powder layer is spread in a bed and selectively melted and joined to previous layer. As the part is sinking into the powder it is being supported by the surrounding powder which allows this method to be used for complex geometries. However, the sinking of the part also leads to the possibility of unbonded powder to be trapped inside of the part. This problem requires careful consideration of print orientation and possible design changes so the unbonded powder can be removed from cavities in the part. This method also experiences stress due to the thermal gradient of the parts that generate thermal stress and may cause internal cracks (Frazier, 2014).

The L-PBF technique is used for the superalloy in this study since it can provide parts with reasonable surface finish and dimensional tolerance.

2.2 Inconel 718

Inconel is a superalloy with nickel (50-55 wt%) and chromium (17-21 %) are the major elements for extreme condition applications. The IN718 is highly weldable, has a resistance to post weld cracking and a yield strength of 1034 MPa (150 ksi) at room temperature and the ability to operate at temperatures of 649°C (1200°F) while maintaining most of its strength (Special Metals, 2007). The combined properties of this alloy and the ability to fabricate complex parts has led to this alloy being used in many applications and industries, for examples liquid fueled rockets, gas turbine engines and cryogenic tanks. The alloy is generally fabricated into the desired part before it goes through its heat treatment process. This allows the part to be machined in its most malleable state since the γ', γ'', and δ precipitates, that formed after the aging process, would be detrimental to a cutting tool (Qingbo Jia, 2013). Two heat treating processes are commonly used: (Special Metals, 2007).

- For high strength. Solution heat treating at 927-1010°C (1700-1850°F) followed by a rapid cooling in water. The next aging next step at 718°C (1325°F) for 8 hours, furnace cooling to 621°C (1150°F) and maintain for 18 hours before air cooling to room temperature.
- For high ductility. Solution heat treating at 1038-1066°C (1900-1950°F) followed by a rapid cooling in water. The following aging step at 760°C (1400°F) for 10 hours, furnace cooling to 649°C (1200°F) for 20 hours before air cooling to room temperature.

2.3 Machinability of Inconel 718

The machinability of L-PBF'ed IN718 is affected by many printing parameters that affects its microstructure: laser power, powder quality, scanning strategy, hatch distance, and layer thickness. Its microstructure is affected by the rapid cooling rate induced by the laser which leads to a fine dendritic cast structure being formed. The dendrite grows parallel with the axis of the build direction. This parallel growth can be attributed to the cooling process of Inconel which cools in the opposite direction of build due to the cooling effects of the substrate (Wang et al., 2011). The L-PBF process leads to a columnar architecture and micropores (Amato et al., 2012), different precipitates (Qingbo Jia, 2013), metallic carbide particles, and Laves phases (Marino et al., 2023). These micropores, precipitates, and particles can lead to machining abnormalities that effect the surface finish and tool life. These changes in microstructure that result in a columnar architecture have been linked to the input laser density and vertical cooling pattern. These vertical cooling directions can lead to the lower portion of the 3D printed part to have a higher hardness value due to those sections going through an age hardening process as they cool slower than the top portions (Qingbo Jia, 2013). This hardness gradient can lead to difficulties when machining at different sections along the part. The changing hardness can lead to different tool wear rates and eventually lead to incorrect dimensions. Some of these microstructure issues can be resolved with a heat treatment to demolish dendrite structures; however, the long and narrow grains still show the build direction of the part and the precipitates are still seen on the grain boundary (Wang et al., 2011). The heat treatment process used to recrystallize the microstructure is an annealing process higher than 593°C (1100°F) (Chlebus et al., 2015). Hot isostatic pressing (HIP) can be used to remove most micropores (Frazier, 2014). It is done inside of a furnace that is enclosed in a pressure vessel where argon gas is used inside this pressure vessel to create the isostatic pressure (Pressure Technology, 2019). This pressure and temperature cause the metal to plastically deform that allows the porosity closure and diffusion to "heal" pores. This results in a higher density for the L-PBF part.

Micromachining of wrought Inconel 718 has been studied. Sredanovic et al. (2017) concluded that a feed of 0.012 mm, depth of cut of 0.02 mm and a cutting speed of 40 m/min were found to be the optimum values for a Ø0.6 mm micro-end-mill when considering cutting forces, channel depths and surface quality of nine different combinations. Ucun et al. (2014), used five different tool coatings (AlTiN, AlCrN, TiAlN+AlCrN, TiAlN+WC/C and diamond-like carbon) and an uncoated tool – the reference for comparison – when machining IN718 in dry cutting conditions. One of the reasons for increasing surface roughness when machining with uncoated tool was the adhesion of chips on the cutting edge, also known as built up edge (BUE). The tool coating protected the tool from wear and BUE forming. The coating that showed the best results was the diamond-like coating while the inferior coatings were the TiAlN+AlCrN and AlCrN due to a chemical reaction between CrN in the coating and IN718. Diamond-like coating prolonged the tool life while producing high machined surface quality of the part.

Minimum quantity lubrication (MQL) has been shown to enhance machinability and tool life when machining 3D printed IN718. The traditional flood cooling uses an excessive amount of coolant to lubricate the tool and workpiece while reducing their temperature. When properly applied, MQL can keep the tool sufficiently lubricated and temperatures lowered without the excess waste. An MQL system uses compressed air to aerosolize the lubricant and then carries it to the tool and part at high speeds as micron sized droplets. Khan et al. (2018) found that an air pressure of 550 kPa (5.5 bar) and a rough-surface nozzle produced the average airborne Coolube oil droplets as small as 5 µm. These smaller droplets effectively lubricated and cooled the tool/chip to produce better surface finish while clearing chips away from a moving microtool. Ucun et al (2014) compared the effect of dry, MQL, and cryogenic cooling of wrought IN718 during micromilling. The MQL provided the best tool performance in terms of tool wear resistance and prevention of BUE formation. However, cryogenic cooling produced the best surface finish. Ji et al. (2021) compared machinability of wrought and as-printed SLM'ed IN718 in dry micromilling. As expected, an increase of tool flank wear and tool diameter reduction were proportional to either cutting speed or chip load; therefore, the surface roughness also increased due to tool degradation. Compressive residual stress resulted after micromilling on both materials; however, the residual stress magnitude on SLM samples were less since it was offset by residual tensile stress due to rapid heating and cooling.

When micromilling DED'ed H13 tool steels, Russell et al. (2022) computed the theoretical average surface finish due to milling with a flat-end milling tool:

$$Ra\_t = \frac{5}{18} \times f_r \times tan \propto \quad (1)$$

Where,

Ra_t : theoretical average surface finish (µm)
f_r : chip load (µm /flute)
α : concavity angle (°)

The authors found that experimental data for surface finish at the beginning of a cut agreed with the theoretical surface finish Ra_t, but then gradually increased to approximately from 3 to 4 times of Ra_t before being leveled. They hypothesized that such slope change was due to the transition of coating layer from fully active to completely being removed by friction at the tool-chip interface.

3. EXPERIMENTS

The samples (15 x 20 x 5 mm) were additively printed with the Renishaw AM250 system. The 15 x 20 mm base surface was on the scanning xy-plane while the 5-mm sample thickness was along the building z-direction. The IN718 powder (50 µm average diameter) was fused with a YAG laser at 160 W power, 110 µm hatching distance in argon gas. Two scanning strategies were employed: The S-blocks were layer-built using the stripe strategy, where laser scanned in alternate 67° direction on adjacent layers; the C-blocks were layer-built using the checkerboard strategy, where laser scanned alternate small squares on a layer. All specimen columns were cut off, perpendicular to the z-axis to separate them from the machine platform, using wire-type electrical discharge machining (wire EDM).

Micromachining was completed on four SLM'ed IN718 samples (named S4, S5, C7, and C9) with a Haas OM2 milling system that was equipped with an 50,000 rpm air spindle. The study used tools of Ø0.5 mm diameter, 2-flute flat end mills provided by Performance MicroTools and coated with either AlTiN or AlTiN/Si_3N_4 under the trade name NanoTek by SwissTek Coatings. All milling operations were performed in MQL provided with a Unist system at 415 kPa (4.15 bar) air pressure and Coolube 2200EP oil. Each IN718 sample was first milled with a ø3.175 mm (ø1/8 in) tool to remove the top rough surface and level it to the xy plane of the milling table. Parallel slots were then micromilled along the 15 mm dimension with a rib of 0.15 mm between slots. Both cutting speed and chip load were varied for different blocks while keeping the axial depth of cut constant at 20 µm. The machining variables were cutting speed, chip load, tool coating and scanning strategy. Each block had four sets of eight slots machined with four different sets of test parameters (Table 1).

Table 1: Parameters for micromilling

Sample	Parameter	First set of 8	Second set of 8	Third set of 8	Fourth set of 8
S4	Coating	AlTiN	NanoTek	AlTiN	NanoTek
	Cutting speed (m/min)	10	10	10	10
	Chip load (µm/tooth)	0.8	0.8	1.2	1.2
S5	Coating	AlTiN	NanoTek	AlTiN	NanoTek
	Cutting speed (m/min)	14	14	19	19
	Chip load (µm/tooth)	1.0	1.0	1.0	1.0
C7	Coating	AlTiN	NanoTek	AlTiN	NanoTek
	Cutting speed (m/min)	14	14	19	19
	Chip load (µm/tooth)	1.0	1.0	1.0	1.0
C9	Coating	AlTiN	NanoTek	AlTiN	NanoTek
	Cutting speed (m/min)	10	10	10	10
	Chip load (µm/tooth)	0.8	0.8	1.2	1.2

After machining, the samples were cleaned to remove any oil residues and contaminates. Each sample was cleaned in an ultrasonic bath while being submerged in isopropyl alcohol for 3 minutes. After cleaning, the samples were handled with sterile tweezers, blew dried with compressed air, and stored in an airtight case. All samples were observed with the Olympus STM7 measuring microscope, scanned using the 3D digital microscope Alicona Infinite Focus G4. Each data set required 48 images to capture the entire tool path. From these scans the roughness average Ra and the slot width were determined along the tool path. The roughness average was calculated over a line distance of 1.5 mm along the slot center line. Both of these parameters had 40 points generated for each data set. The slot width was taken at the beginning of the first slot and in the middle of the eight slots. This generated a total of 9 data points that followed the tool path.

After the roughness and slot width images were captured, the samples were scanned with the Vegas scanning electron microscope (SEM) and analyzed using an integrated energy dispersive X-ray (EDS) system. These scans were done on the machined surfaces and any the inclusions that were found during the previous microscope scans to determine their chemical compositions. Fatigue testing was performed in a parallel study on the same L-PBF'ed IN718. The microstructure of fatigue fractured surfaces was compared with that on micromilled surfaces.

4. RESULT AND DISCUSSION

4.1 Microstructure

Machinability is traditionally evaluated by assessing tool degradation, i.e., tool wear or the changes in tool geometry. Removing a microtool in micromachining for tool measurement and then precisely remount it again to continue a test, however, is very time consuming and a technical challenge to maintain the same machining parameters (depth of cut, tool position….) This study analyzes the quality of micromilled slots as an indication of tool degradation. Both surface finish and micromilled slot dimension were measured precisely with the Alicona microscope. Microstructure was observed to complement the surface finish data since it affected tool performance.

Figure 1 shows the top view of micromilled slots. The microstructure of wrought IN718 is homogeneous, but the microstructure of L-PBF'ed IN718 clearly shows different phases: the irregular phases surrounded by the metallic matrix.

The phases, sheared by a micromilling tool, exhibited brittle fracture and seemed to form near an edge of a block (Fig. 1a), perhaps due to faster cooling rate compared to the central material. Energy dispersive X-ray analysis revealed high carbon concentration and reduced content of Ni, Cr, Fe, and Nb compared to those in the matrix (Fig. 2 and Table 3). These intermetallic carbide phases were different from the Nb-rich Laves phases in IN718 (Zhao et al., 2020).

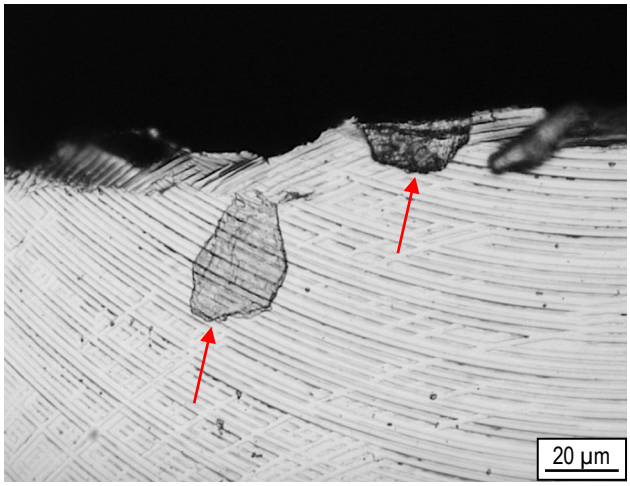

Figure 1a – Carbide particles (at arrows) in IN718 matrix. Machined surface of S4 specimen.

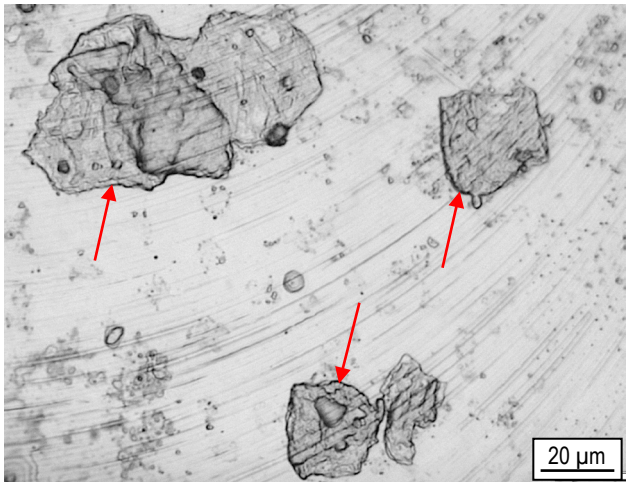

Figure 1b – Carbide particles (at arrows) in IN718 matrix. Machined surface of C9 specimen.

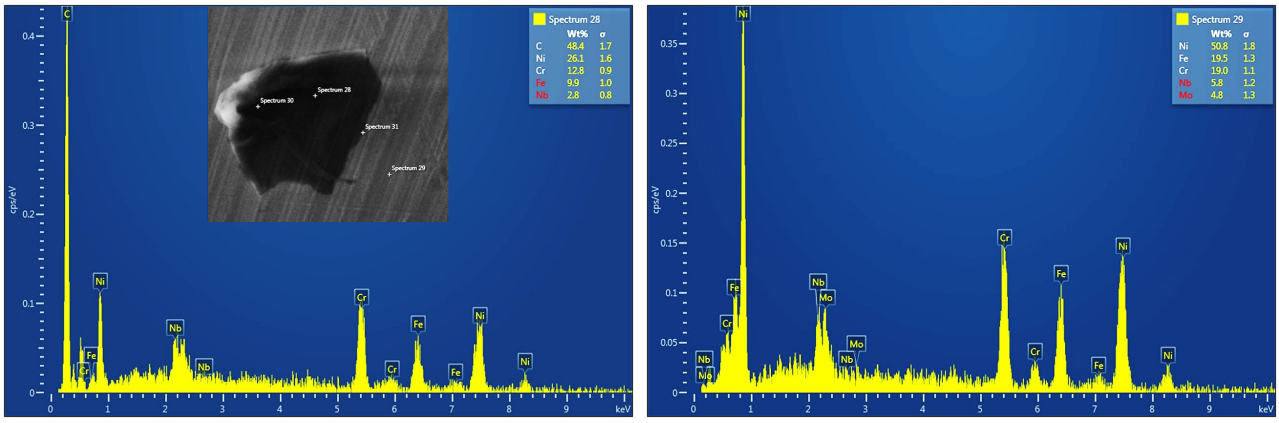

Figure 2 – EDS spectrums at a point inside (left) and outside (right) of the carbide particle.

Table 3. Element analysis of the carbide phase and its surrounding

Element	C (wt%)	Ni	Cr	Fe	Nb	Mo	Ti	Al
Carbide	48.4	26.1	12.8	9.9	2.8			
Matrix		50.8	19.0	19.5	5.8	4.8		
IN718 *	0.08 max	50-55	17-21	13-24	4.75-5.50	2.80-3.30	0.65-1.15	0.20-0.80

* www.specialmetal.com

Assuming higher hardness than the matrix, these metallic carbides would damage the fragile cutting edges of a microtool. Microscopic observation showed shattered carbide phases smearing on the machined surface and degrade both the tool and resulted surface finish (Fig. 3). Fatigue fracture surfaces also showed the brittle nature of these metallic carbides (Fig. 4).

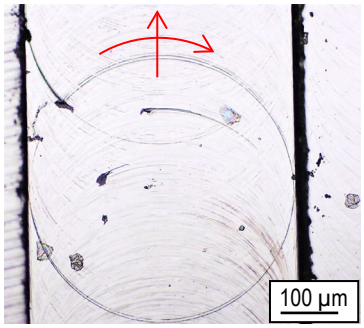

Figure 3 – Smearing of broken carbide particles on machined surface. The arrows indicate tool feed and tool rotation directions. Sample S4.

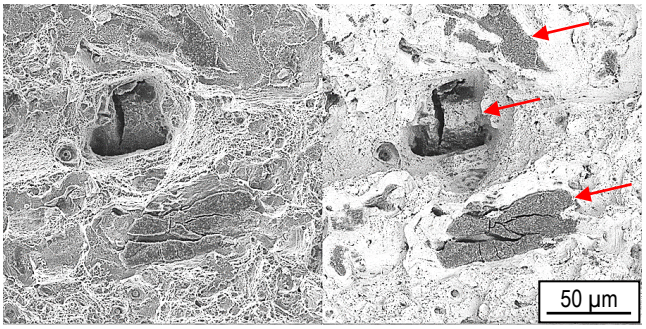

Figure 4 – Secondary (left) and back-scattered electron (right) images of brittle carbide particles (at arrows) after fatigue testing.

4.2 Surface finish

Surface finish was measured along a slot center line for all slots. Typical plots of surface finish for all slots are shown in Fig. 5 for both scanning strategies and tool coatings. Equation (1) assumes ideal milling conditions with new tool and homogeneous workpiece material; the theoretical surface finish calculation is based on the tool-end geometry (concavity angle) and the chip load. Measured surface finish commonly is higher than the theoretical value due to tool wear, tool coating defects, vibration, lack of lubrication, built-up-edge formation, and inhomogeneity of workpiece material. Using an end milling tool with 3° concavity angle, the effects of chip load on surface finish is calculated using equation (1) and tabulated below.

Table 2. Effect of chip load on theoretical surface roughness

f_r (µm /flute)	0.8	1.0	1.2	5	10
Ra_t (µm)	0.01165	0.01456	0.01747	0.07279	0.14558
4 x Ra_t (µm)	0.0408	0.0510	0.0611	0.2548	0.5095
100 x Ra_t (µm)	1.165	1.456	1.747	7.279	14.558

Extrapolation of measured data in Fig. 5 reasonably agreed with the theoretical surface finish of 0.01 µm when using 1 µm chip load (Table 2). The steep increment of surface finish was due to the poor machinability of IN718 superalloy, and the presence of hard and brittle carbide particles. Recall that 15x25 mm blocks were printed for this study, and each milling slot is 15 mm long, and carbide particles tent to form near the circumference of the block due to fast cooling. A microtool would encounter more carbide particles at the beginning or end of a slot, i.e., smearing of shattered carbide particles could be expected at milling distance in multiple of 15 mm. In Fig. 5, a "*" next to data point with unusually high surface finish are shown.

In all cases, the slopes of surface finish lines seemed to level after 15 mm milling distance (the length of very first slot) regardless of cutting speed, chip load, tool coating, or scanning strategies. When micromilling the as-printed and homogeneous H13 steel, the surface finish data leveled approximately beween 3 to 4 times the theoretical value (Russell et al., 2022), but data from this study leveled at 100 times the theoretical value to 1.5 µm Ra (Table 2). So, surface finish would not be a precise metric to evaluate machinability of the as-printed and inhomogeneous IN718.

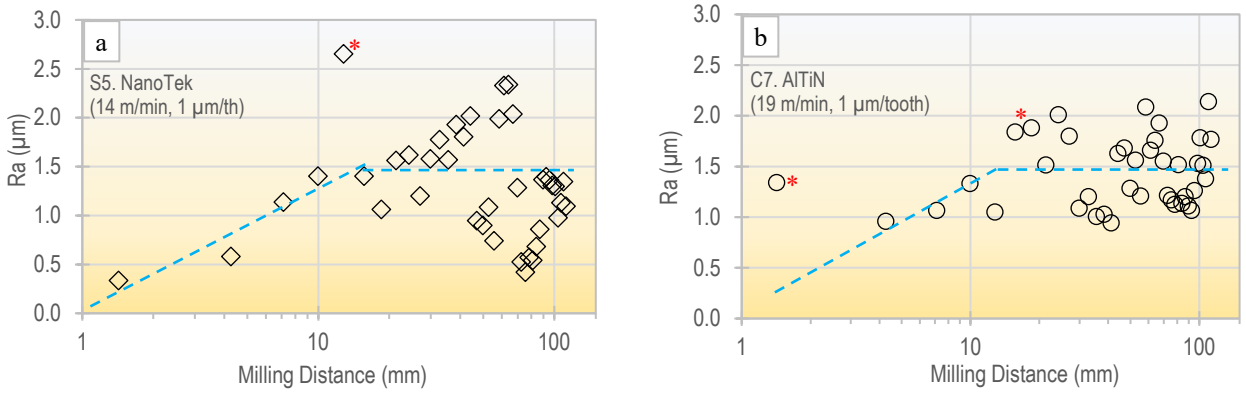

Figure 5 – Surface finish of micromilled slots on (a) sample S5 and (b) sample C7.

4.3 Slot width

Degradation of a micromilling tool affects surface finish and geometry of a machined slot. Since burr is generated on both sides and on top of a machined slot, the slot width at bottom of a slot is measured for indirect assessment of the cutting tool. Figures 6 presents and compares the changes of slot widths with milling distance and the effects of tool coating, scanning strategies, as well as machining parameters.

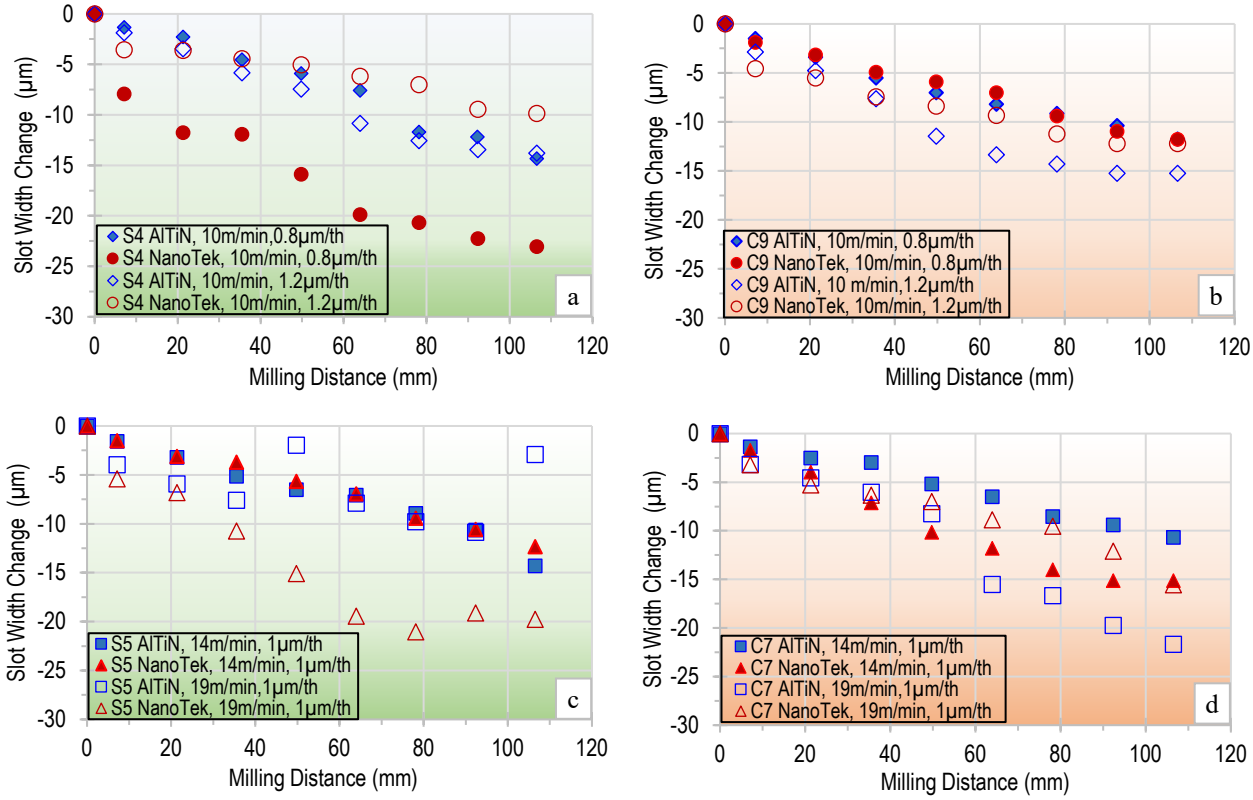

Figure 6 – Tool wear affects the slot widths on (a) sample S4, (b) sample C9, (c) sample S5, and (d) sample C7.

Due to the presence of "random" carbide particles that can damage a microtool, the assessment would:

i) Exclude data with abrupt change of slot width
ii) Exclude data beyond 40 mm when the coating layer, typically 1-2 µm thick, is completely worn out

The slot width data suggested that:

- A higher chip load (1.2 µm/tooth) enhanced tool wear and promoted faster slot width change (Figs. 6a, b)
- A faster cutting speed (19 m/min) also deteriorated tool faster and caused faster slot width change (Fig. 6c, d)
- There was no statistical difference for tool coating performance, either NanoTek or AlTiN, when micromilling L-PBF'ed IN718. Perhaps the hard and brittle intermetallic carbide phases could damage both coatings equally.
- Slot width data for sample C, produced with checkerboard scanning, seemed to be more consistent than those with S (stripe) scanning. Perhaps spreading of deposited materials in checkerboard strategy would provide more uniform heat distribution in the workpiece, therefore, resulted in more uniform microstructure and less residual stress level. Two data sets were discarded: sample S4, NanoTek coated tool, 10 m/min speed, 0.8 µm/tooth chip load; and sample S5, NanoTek coated tool, 19 m/min speed , 1 µm/tooth chip load. The data showed unusual slot width changes on samples S4 and S5 (Figures 6a and 6c) suggested that the tools may be damaged due to colliding and shearing of the hard carbide particles.

Machinability study was hindered by the hard carbide phases in L-PBF'ed IN718. High density carbide particles were seen near the part corner where heat loss is the greatest (Figs. 1a and 7a). The part boundary was also covered with partially welded powders that could be contaminated from recycled powders (Fig. 7b). Perhaps an appropriate heat treatment to dissolve the carbide phases and transform the IN718 into a more homogeneous material should be performed prior to micromilling. Removal of both top materials (xy-plane) and the surrounding peripherals (xz and yz planes) should be the requirement before machinability study.

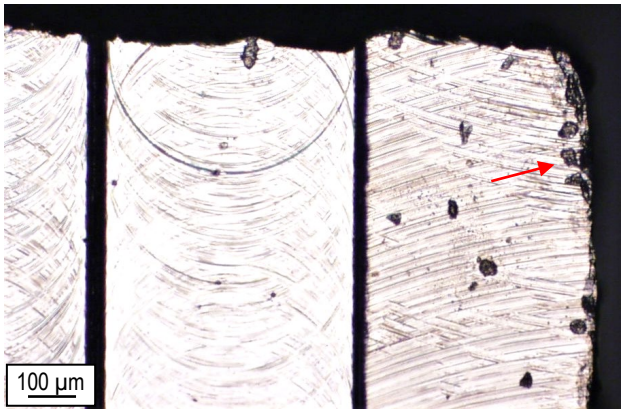

Figure 7a – High density of carbide particle (at arrows) near the block boundary. S-sample.

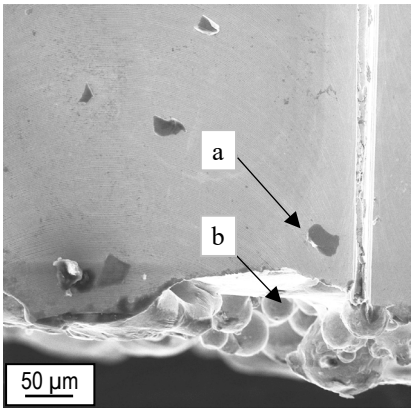

Figure 7b – (a) Carbide particles and (b) partially-welded IN718 powder particles at the part boundary. S-sample.

5. CONCLUSIONS AND RECOMMENDATIONS

Micromilling of laser powder bed fused (L-PBF) Inconel 718 was studied. The experimental study found that:

1) High density of carbide particles was found near the part boundaries and isolated particles were seen within the part volume. These hard particles were sheared and smearing on a surface, therefore, they degraded the surface finish and chipped the tools' fragile cutting edges.
2) The was no significant difference of tool performance when comparing AlTiN or NanoTek ($AlTiN/Si_3N_4$) coating. The surface finish data were affected by smearing of broken carbide particles and chipped tools. The average surface finish data were 100 times higher than the theoretical value.
3) Slot width measurement was implemented to evaluate tool performance and machining parameters. Aggressive machining parameters (high cutting speed or chip load) deteriorated a tool and reduced the micromilled slot width. The widths were reduced approximately 15 µm after 100 mm milling distance.
4) Scanning strategies also affected the microstructure and machinability. Laser scanning in checkerboard pattern seemed to have less concentrated carbide particles and produced more consistent machining data than samples with stripe scanning strategy.

Future work on additively manufactured IN718 should minimize, if not eliminate, the effects of contamination and detrimental carbide particles before machinability study. The recommended steps include:

i) Dissolving the carbide particles by a suitable heat treatment process.
ii) Removing the part boundaries before machinability study. Wire-type electrical discharged machining or slow grinding would be recommended.

6. ACKNOWLEDGEMENTS

The authors thank TAMU Imaging Center Core Facility (RRID:SCR_022128) for SEM imaging, Performance Micro Tools for the microtools, and SwisTek Coating for providing different tool coatings. The kind support from KGSBO for the additively manufactured samples is much appreciated.

7. REFERENCES

Amato, K.N., Gaytan, S.M., Murr, L.E., Martinez, E., Shindo, P.W., Hernandez, J., Collins, S., and Medina, F., 2012. Microstructures and mechanical behavior of Inconel 718 fabricated by selective laser melting. Acta Materialia. 60, pp. 2229-2239.

Anthony Marino, Shyam Balasubramanian, Matthew Carl, Mike Corliss, and Wayne Hung, 2023. Effects of Print Parameters and Heat Treatment on Microstructure of Inconel 718 Fabricated by Laser Powder Bed Fusion. Journal of Advanced Manufacturing Technology, pp. 1-20. https://doi.org/10.1007/s00170-022-10773-4.

Chlebus, E., Grubuer, K., Kuznicka, B., Kurzac, J., and Kurzynowski, T., 2015. Effect of heat treatment on the microstructure and mechanical properties of Inconel 718 processed by selective laser melting. Materials Science & Engineering A. 639, pp. 647-655.

Frazier, W.E., 2014. Metal Additive Manufacturing: A Review. J. Materials Eng. Performance. 23(6), pp. 1917-1928.

Gibsin, I., Rosen, D., and Stucker, B., 2015. Additive Manufacturing Technologies, second ed. Springer, New York, ch. 5,7 and 10.

Hansong Ji, Munish Kumar Gupta, Qinghua Song, Wentong Cai, Tao Zheng, Youle Zhao, Zhanqiang Liu, and Danil Yu Pimenov, 2021. Microstructure and machinability evaluation in micro milling of selective laser melted Inconel 718 Alloy. Journal of Materials Research and Technology, 14:348-362.

Khan W.A., Hoang N.M., Tai B., and Hung W.N.P., 2018. Through-tool minimum quantity lubrication and effect on machinability. J. Manufacturing Processes. 34, pp. 750-757.

Pressure Technology, 2019. https://www.pressuretechnology.com/about-hip.php

Qingbo Jia, D.G., 2013. Selective laser melting additive manufacturing of Inconel 718 superalloy part: Densification, microstructure and properties. J. Alloys Compounds. 585, pp. 713-721.

Russell A., Suri S.B., Ribeiro K.S.B., Coelho R.T.2, De Freitas S.A., Gomes M.C., Da Silva M.B., De Oliveira D., and Hung N.P.W., 2022. Micromilling H13 Tool Steel and Tool Life Criteria for Coated Microtools, pp. 3-7, ISBN-13: 978-981-18-5180-3. The 5th World Congress on Micro and Nano Manufacturing, Leuven, Belgium, September 2022.

Special Metals, 2007. http://www.specialmetals.com/assets/smc/documents/inconel_alloy_718.pdf

Sredanovic, B., Lakic, G., Kramar, D., and Kopac, J., 2017. Study of the Machinability Characteristics of Inconel 718 Super Alloy During Micro-Milling. Proceedings of 5th International Conference on Advanced Manufacturing Engineering and Technologies, pp. 375-385.

Ucun I., Aslantas K., and Bedir F., 2014. The effect of minimum quantity lubrication and cryogenic pre-cooling on cutting performance in the micro milling of Inconel 718. Proc IMechE Part B: J Engineering Manufacture 1–10, IMechE 2014J. DOI: 10.1177/0954405414546144.

Ucun I., Aslantas K., Gokce B., and Bedir F., 2014. Effect of tool coating on materials on surface roughness in micromachining of Inconel 718 super alloy. J. Engineering Manufacture. 228(12), pp. 1550-1562.

Wang Z., Guan K., Gao M., Li X., Chen X., and Zeng X., 2011. The microstructure and mechanical properties of deposited-IN718 by selective laser melting. J. Alloys Compounds. 513, pp. 518-523.

Xiaohong Lu, Xiaochen Hu, Zhenyuan Jia, Mingyang Liu, Song Gao, Chenglin Qu, and Steven Y. Liang, 2018. Model for the prediction of 3D surface topography and surface roughness in micro-milling Inconel 718. J. Advanced Manufacturing Technology, 94:2043–2056. DOI 10.1007/s00170-017-1001-y.

Yanan Zhao, Kai Guan, Zhenwen Yang, Zhangping Hu, Zhu Qian, Hui Wang, and Zongqing Ma, 2020. The effect of subsequent heat treatment on the evolution behavior of second phase particles and mechanical properties of the Inconel 718 superalloy manufactured by selective laser melting. Materials Science & Engineering A 794 139931.

8. RESPONSIBILITY NOTICE

The authors are the only responsible for the printed material included in this paper.